

Laser Acceleration of Highly Energetic Carbon Ions Using a Double-Layer Target Composed of Slightly Underdense Plasma and Ultrathin Foil

W. J. Ma,^{1,3,*} I Jong Kim,^{2,4,†} J. Q. Yu,¹ Il Woo Choi,^{2,4} P. K. Singh,² Hwang Woon Lee,² Jae Hee Sung,^{2,4} Seong Ku Lee,^{2,4} C. Lin,¹ Q. Liao,¹ J. G. Zhu,¹ H. Y. Lu,¹ B. Liu,⁵ H. Y. Wang,⁶ R. F. Xu,¹ X. T. He,¹ J. E. Chen,¹ M. Zepf,^{7,8} J. Schreiber,^{3,5} X. Q. Yan,^{1,9,‡} and Chang Hee Nam^{2,10,§}

¹State Key Laboratory of Nuclear Physics and Technology, and Key Laboratory of HEDP of the Ministry of Education, CAPT, Peking University, Beijing 100871, China

²Center for Relativistic Laser Science, Institute for Basic Science, Gwangju 61005, Korea

³Fakultät für Physik, Ludwig-Maximilians-Universität München, D-85748 Garching, Germany

⁴Advanced Photonics Research Institute, Gwangju Institute of Science and Technology (GIST), Gwangju 61005, Korea

⁵Max-Planck-Institute für Quantenoptik, D-85748 Garching, Germany

⁶School of Environment and Chemical Engineering, Shanghai University, Shanghai 200444, China

⁷Helmholtz-Institut-Jena, Fröbelstieg 3, 07743 Jena, Germany

⁸Department of Physics and Astronomy, Centre for Plasma Physics, Queens University, Belfast BT7 1NN, United Kingdom

⁹Collaborative Innovation Center of Extreme Optics, Shanxi University, Taiyuan, Shanxi 030006, China

¹⁰Department of Physics and Photon Science, GIST, Gwangju 61005, Korea



(Received 20 November 2017; published 10 January 2019)

We report the experimental generation of highly energetic carbon ions up to 48 MeV per nucleon by shooting double-layer targets composed of well-controlled slightly underdense plasma and ultrathin foils with ultraintense femtosecond laser pulses. Particle-in-cell simulations reveal that carbon ions are ejected from the ultrathin foils due to radiation pressure and then accelerated in an enhanced sheath field established by the superponderomotive electron flow. Such a cascaded acceleration is especially suited for heavy ion acceleration with femtosecond laser pulses. The breakthrough of heavy ion energy up to many tens of MeV/u at a high repetition rate would be able to trigger significant advances in nuclear physics, high energy density physics, and medical physics.

DOI: 10.1103/PhysRevLett.122.014803

Dense, energetic heavy ion bunches with an ultrashort duration are in high demand for high-energy-density physics and nuclear astrophysics [1,2]. Near the source, laser-driven ion acceleration can deliver exceptional ion bunches 10^{10} times denser than classically accelerated ion bunches [3,4], which highlights its application prospect in related fields. So far, energetic heavy ions up to 80 MeV/u have been generated through breakout afterburner [5,6] and relativistic transparency [7,8] acceleration schemes. But both of these schemes require expensive 100s J level long-pulse lasers which are still unable to operate at a high repetition rate. Femtosecond laser pulses have been successfully applied in proton acceleration with the advantages of lower request on laser energy and Hertz-level repetition rate [9]. However, heavy ion acceleration with femtosecond pulses has not achieved the same success. The maximum energy per nucleon is still no more than 25 MeV/u, mostly only a few MeV/u [9–14], inefficient to overcome the Coulomb barrier to excite nuclear reactions or isochorically heat bulk matters to a warm dense state.

For femtosecond pulses, target normal sheath acceleration (TNSA) [15] and radiation pressure acceleration (RPA) [16,17] are the most widely employed schemes.

In the TNSA scheme, the acceleration field (sheath field), established by laser-produced dilute thermal electrons, is easily diminished by contaminated protons and poorly ionized heavy ions which appear at the beginning of the interaction. Thus the acceleration of highly ionized heavy ions is strongly suppressed [18–21]. By completely removing the protons in the contamination layer, the energy of the heavy ions can be improved to, in the best cases, a few MeV/u [18,19,21], which is still much lower than the maximum proton energy of 85 MeV achieved in the TNSA scheme [22]. Compared to TNSA, RPA using nanometer-thin foils as targets has been proven more beneficial to accelerating heavy ions due to the fact that the majority of the bulk electrons in the targets are displaced by the radiation pressure. In particular, quasimonoeenergetic ions can be obtained by entering the light-sail RPA regime when circular polarized pulses and matching ultrathin foils are used. Experimental results show that carbon ions up to 25 MeV/u can be generated in the light-sail RPA regime [23]. Simulations predict that highly energetic heavy ions can be generated by using compound targets at an intensity above 10^{21} W/cm² [24,25]. The major problem at the current intensity for RPA is the fast decline of the

acceleration field after laser reflection and unwanted early termination of acceleration due to plasma instability [26,27]. To generate highly energetic heavy ions, increasing the on-target laser intensity, or prolonging the acceleration time, is essential. Recently, a plasma-lens-enhanced RPA (PLE RPA) scheme has been realized [28,29] by enhancing the on-target intensity using a few- μm -thick and slightly overdense plasma (SOP) slab as a plasma lens. Significant enhancement of carbon energy is observed. But 30%–50% of the pulse energy was lost in the SOP without significant contribution to the ion acceleration process.

In this work, we demonstrate the realization of a cascaded acceleration (CA) scheme especially suited for heavy ions. It happens when a laser pulse is focused on a target composed of a homogeneous, tens-of- μm -thick, slightly underdense plasma (SUP) slab in front of an ultrathin foil. Figure 1(a) schematically illustrates the scheme. The density of the SUP is in the range of 0.1 to $1n_c$ to ensure that direct laser acceleration, instead of

wakefield acceleration, happens [30–32], where $n_c = m_e \omega^2 \epsilon_0 / e^2$ is the critical density of the plasma. In the SUP, the electrons are trapped in the plasma channel by an electrostatic field and a self-generated magnetic field, and in-phase accelerated by the laser field to an energy far beyond the ponderomotive limit [33]. As the forward velocities of these “superponderomotive electrons” are lower than the group velocity of the laser pulse, they form a dense and energetic electron flow behind the pulse. Once the laser pulse, self-steepened in SUP and followed by the electron flow, arrives at the ultrathin solid foil, ions residing in the foil undergo radiation pressure acceleration at first, then cascaded acceleration in a long-lifetime sheath field dominated by the superponderomotive electron flow. The superiority of CA is that the initial RPA stage gives rise to an efficient ionization and ejection of highly ionized ions, and the enhanced TNSA stage thereafter ensures a sufficiently long acceleration time. Experimental results show that carbon ions with energy up to 48 MeV/u can be generated by using double-layer targets, which is, to our knowledge, about 2 times that of the previous record obtained by using femtosecond lasers.

The experiments were performed using the petawatt Ti:sapphire laser facility at Center for Relativistic Laser Science (CoReLS) of the Institute for Basic Science (IBS) in Korea. After a recollimating double plasma mirror (DPM) system, 33-fs *s*-polarized laser pulses with energy of 9.2 J were focused to spots of 4.5 μm diameter (FWHM) using a $f/3$ off-axis parabolic mirror, resulting in a peak intensity of $5.5 \times 10^{20} \text{ W/cm}^2$, corresponding to a relativistic normalized vector potential of $a_0 = eE/m_e c \omega \approx 16$. After the DPM, the contrast of the laser pulses was about 3×10^{-11} at 6 ps before the main pulse, which is good enough to avoid the premature expansion of the nanotargets before the arrival of the main pulse. The incident angle was 2.4° , and the ion energy spectra were measured with a Thomson parabola (TP) placed in the direction of the laser axis. The TP was equipped with a microchannel plate (MCP) with a phosphor screen to convert the ion signal to an optical signal imaged by a 16-bit CCD. The absolute response of the MCP was calibrated following the literature [34]. A 6-mm-thick tungsten plate with a 375- μm iris was used as the ion collimator in front of the TP, corresponding to the acceptance angle of 3.5×10^{-8} sr. Bright and stable zero points, on top of halos that resulted from secondary radiation from the collimator, were observed on the CCD as shown in Fig. 1(b). The energy measurement error of the TP, estimated by considering the linewidth of the ion trace and the spatial resolutions of the MCP and CCD, was about ± 2.2 MeV for 60-MeV protons and ± 3.3 MeV/u for 50 MeV/u C^{6+} .

The SUP layer of the double-layer targets was made of carbon nanotube foam (CNF) [35]. Behind the CNF, a nanometer-thin diamondlike carbon (DLC) [36] foil was attached, in which only a minute amount of protons or

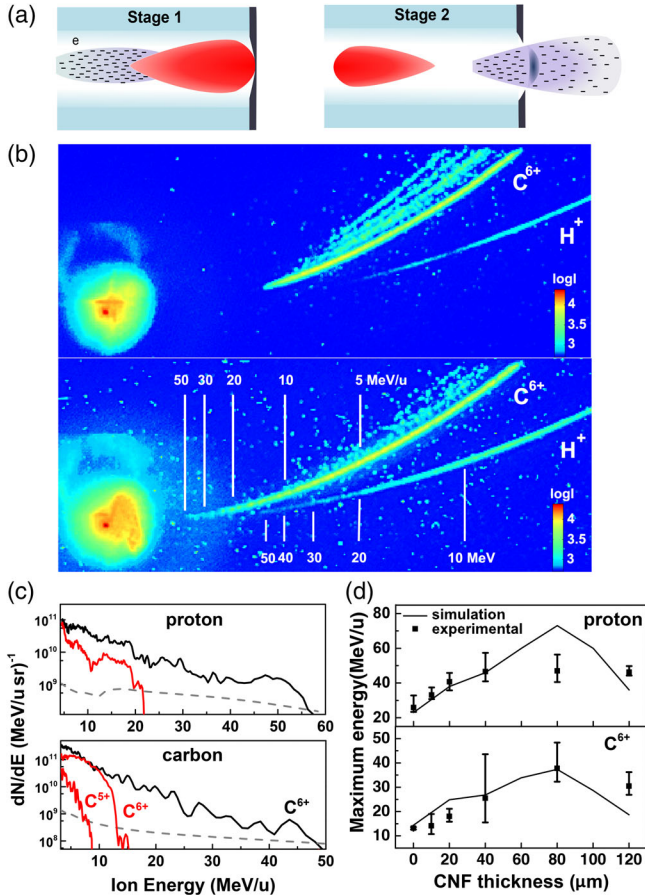


FIG. 1. (a) Schematic drawing of the cascaded acceleration process. (b),(c) Raw data and ion spectra obtained from a 20-nm DLC target [upper image in (b), red lines in (c)] and a double-layer target with 80 μm CNF [lower image in (b), black lines in (c)]. The dashed lines in (c) show the detection threshold. (d) The dependence of the maximum proton or carbon energy on the thickness of the CNF layer.

oxygen lie in the contamination layer (for details about the targets, see Supplemental Material [37]). The targets were not treated by laser heating or other proton-removal methods. In the experimental campaign, the bulk density of the employed CNF was $3 \pm 1.5 \text{ mg/cm}^3$, corresponding to an electron density of $0.4 \pm 0.2n_c$ if carbon atoms were fully ionized. The thickness of CNF was varied from 0 to $120 \mu\text{m}$ in the experiments, while the DLC was fixed to 20 nm for all the targets. The raw data and ion spectra of 2 shots, obtained from a single-layer 20-nm DLC target and from a double-layer target with $80 \mu\text{m}$ CNF are shown in Figs. 1(b) and 1(c), respectively. Two features are obvious: (1) the energy and the number of carbon and proton ions obtained from the double-layer target are remarkably higher than those from the single-layer target and (2) $6+$ is the *only* dominant charge state of carbon ions for the double-layer target, while multiple charge states were observed in the case of the single-layer target. For further confirmation, an additional 53 shots by varying the thickness of the CNF were made in the campaign. It turned out that the above features were repeatedly observed. The missing low charge states of carbon ions for the double-layer targets implies that the ionization processes were not evolving but abrupt and complete. The maximum energies of protons and of C^{6+} are plotted as a function of CNF

thickness in Fig. 1(d), where the error bars reflect the shot-to-shot fluctuation and the dots are the arithmetic means. A strong dependency of ion energy on the CNF thickness is observed. The optimal thickness is $80 \mu\text{m}$ for carbon acceleration, resulting in a maximum 48 MeV/u . The solid lines in Fig. 1(d) depict the numerical simulation results (for simulation parameters, see below), which fit to the experimental results very well.

To illustrate the physics, 2D particle-in-cell simulations were performed using the EPOCH2D [38] code. The simulation window was $W_x \times W_z = 160 \times 40 \mu\text{m}^2$ with the cell size of $dx = dz = 10 \text{ nm}$. The laser pulse traveled along x from the left side with a central wavelength of 800 nm and \sin^2 temporal profiles. Its peak laser intensity, focused spot, and duration is $5.5 \times 10^{20} \text{ W/cm}^2$, $4.5 \mu\text{m}$, and 33 fs , respectively, the same as in experiments. The electron density of the CNF/DLC layer was $0.2n_c/50n_c$. The thickness of the DLC layer in simulation was set to 200 nm to ensure its areal density was the same as that of the 20-nm unionized DLC. The thickness of the CNF varied from 0 to $120 \mu\text{m}$.

Snapshots of E_y , E_x , and $(\gamma - 1)n_e$ at four different times are shown in Fig. 2(a), where E_y and E_x are the electric fields and γ and n_e are the Lorentz factor and the density of

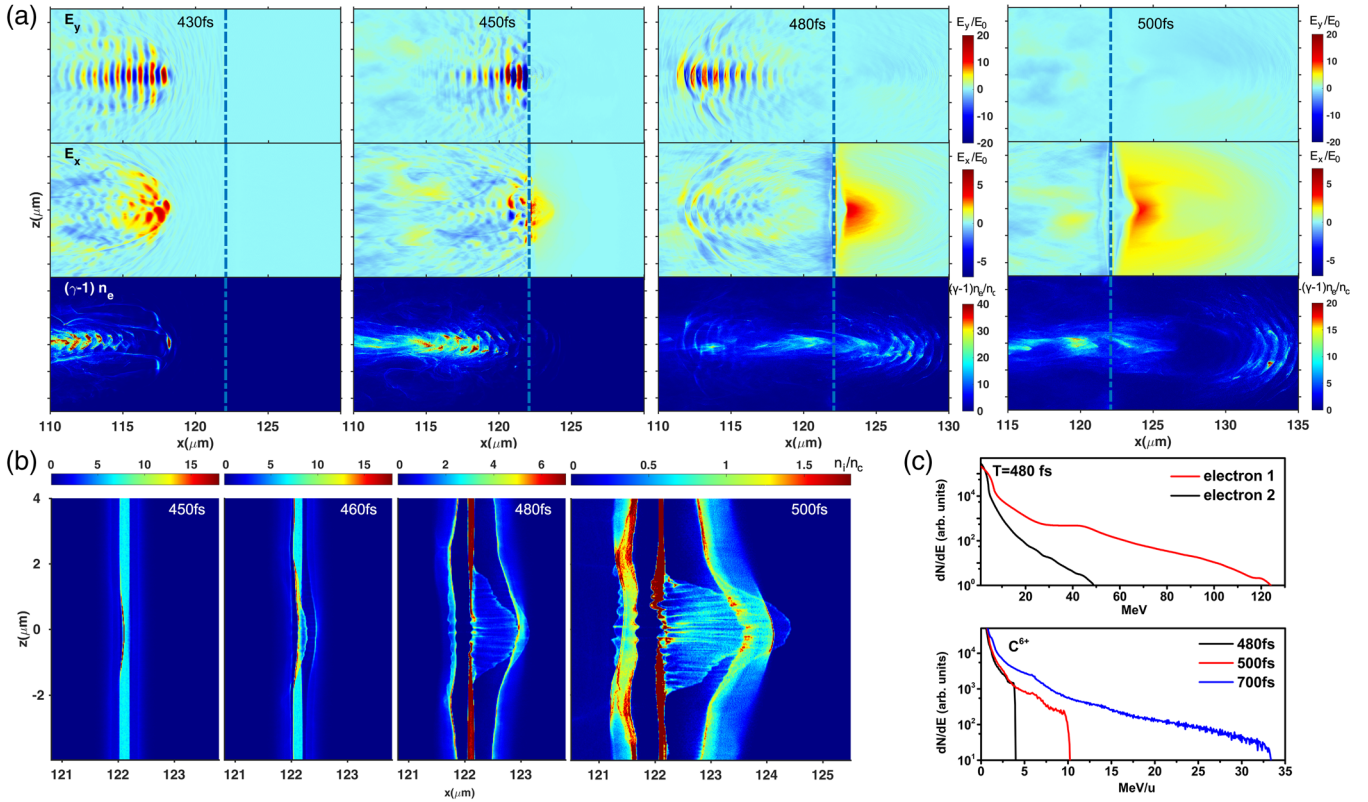


FIG. 2. (a) Snapshots of transverse electric field (E_y), longitudinal electric field (E_x), and the energy density $[(\gamma - 1)n_e]$ of electrons from CNF at different times. (b) Snapshots of the density of C^{6+} . (c) Energy spectra of electrons in CNF (red line) and in DLC (black line) at $T = 480 \text{ fs}$, and the C^{6+} spectra at different times.

electrons from the CNF, respectively. At $T = 430$ fs, the laser pulse has not arrived at the solid foil (the blue dash-dotted line at $122 \mu\text{m}$). After propagating $\sim 55 \mu\text{m}$ in CNF, the pulse duration (FWHM) is reduced from 33 to 15 fs with a steep rising edge due to relativistic nonlinearity in the SUP. The intensity is moderately enhanced by 50%, in contrast to the case of PLE RPA, where the pulse is strongly self-focused. A major portion of the laser energy is coupled to superponderomotive electrons in the near-critical-density channel through direct laser acceleration [33,39], forming a high-energy-density electron flow behind the pulse. At $T = 450$ fs, the pulse has been at the solid foil for 5 fs. Electrons in the foil are piled up by the radiation pressure, resulting in a strong and localized charge separation field, which piles up ions as well and accelerates them forward. Figure 2(b) shows the density of C^{6+} at different times. It can be seen that ions in the foil are piled up at 450 fs with a density rise of a factor of 2, and then a large portion of them were ejected from the foil at 460 fs. At $T = 480$ and 500 fs, the laser pulse has been completely reflected away, but the accelerating field is still very strong. The dominant ion acceleration process is TNSA. The sheath field is established by the superponderomotive electron flow from the SUP and the thermal electrons from the DLC. The energy spectra of the two kinds of electrons are shown in Fig. 2(c). It can be seen that both the number and the energy of the superponderomotive electrons are much higher than those of the thermal electrons. Thus, the sheath acceleration stage is dominated by the superponderomotive electrons, which is remarkably different from the hybrid-RPA scheme where the sheath acceleration is purely due to thermal electrons [11,40]. Simulation results show that such a sheath field is very strong and can last over 200 fs, which is crucial for achieving efficient acceleration of heavy ions with low charge-to-mass ratio. The energy spectra shown in Fig. 2(c) indicate that carbon ions gain most of their energy in the TNSA stage. From the energy conversion point of view, the TNSA stage plays the dominant role in CA (see Supplemental Material [37]). Nevertheless, the RPA stage is still important because it leads to an efficient ionization and injection of heavy ions at the beginning of the acceleration process.

As demonstrated in the experiments, there is an optimal thickness of the SUP layer for ion acceleration. Around this thickness, a significant amount of pulse energy is converted into electron flow and eventually contributes to the sheath field acceleration. Meanwhile, the remaining pulse is strong enough to displace the bulk electrons and eject ions. This is confirmed by simulations in Fig. 3(a) by tracking the energy gain rate (EGR) of the most energetic carbon ions. In the case of a single foil target without SUP, the EGR starts to rise after the laser pulse arrives at 425 fs, then peaks at about 480 fs when the pulse is reflected away, and quickly declines afterwards. In contrast, for the double-layer target with $60 \mu\text{m}$ CNF, the steepened laser pulse

arrives at the foil at 445 fs. The corresponding EGR rises with a higher speed and reaches a similar value when the pulse is reflected. After that, the EGR continuously grows up until 500 fs, when the majority of the superponderomotive electron flow passes through the foil. If the CNF layer is too thick, for example, $120 \mu\text{m}$, the laser pulse is seriously depleted and filamented [41] before it reaches the DLC. The ions are accelerated merely by the sheath field without the RPA stage. For a comparison to the PLE-PRA regime, a simulation by setting the electron density of CNF to $2n_c$ and thickness to $6 \mu\text{m}$ was performed as well and presented in Fig. 3(a). The tenfold increment of the CNF density to slightly overdense results in stronger self-focusing but without a long superponderomotive electron flow. As a result, although the EGR in the RPA stage (before 480 fs) is higher, the final ion energy is lower compared to $0.2n_c$.

Besides the length and density of the SUP layer, simulations reveal that the thickness of the DLC foil imposes significant influence on the ion acceleration as well. Figure 3(b) shows the dependence of the maximum C^{6+} energy on the thickness of the DLC foils. In the case of $0.2n_c$ SUP, the optimal DLC thickness is 5 nm, and the maximum carbon energy varies little for 10–100 nm DLCs and eventually drops to 27 MeV/u for $1 \mu\text{m}$ DLC. Such a dependency is different from the case of $2n_c$, where the optimal thickness is 10 nm and the maximum C^{6+} energy quickly drops to 12 MeV/u. The simulation results clearly demonstrate the importance of using an ultrathin foil behind the foam, so that the RPA stage can efficiently eject and preaccelerate heavy ions. This has been proved by previous experimental studies where foam-coated micrometer-thick metal foils were shot at laser intensity close to ours, where the energy of the heavy ions was no more than 11 MeV/u [42,43]. As a comparison, the results from

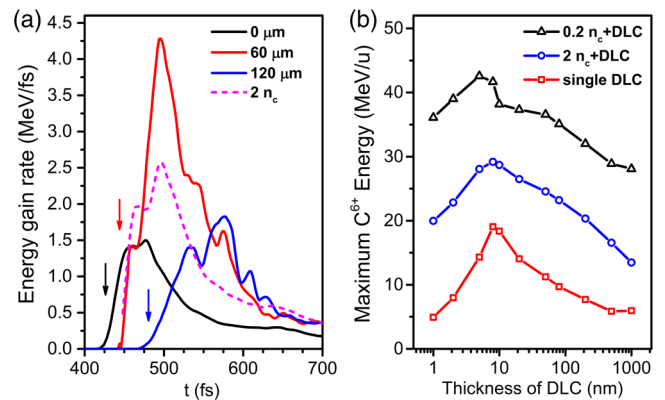


FIG. 3. (a) Energy gain rate (MeV/fs) of C^{6+} ions as a function of time for targets with different CNF layers obtained from simulations. The arrows show the arrival instant of the laser pulses for different cases. (b) The dependence of maximum C^{6+} energy on the thickness of DLC for single DLC targets and double-layer targets obtained from simulations.

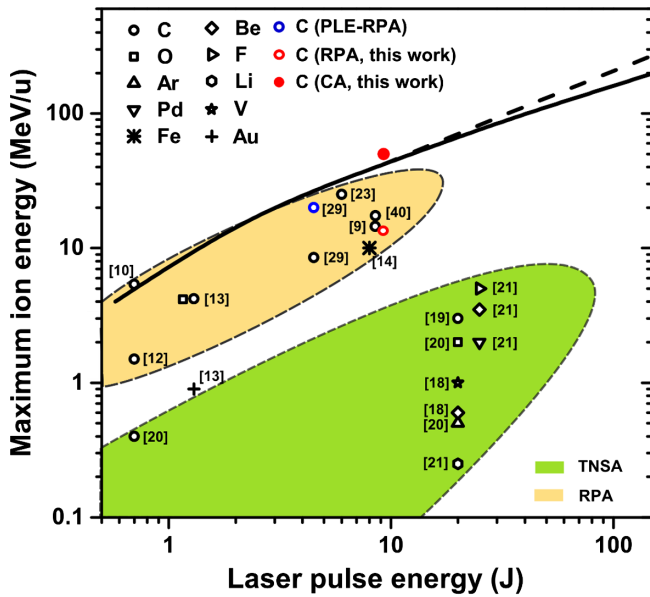


FIG. 4. Summary of reported experimental results (shown by the reference number) and scaling of carbon ions in cascaded acceleration scheme.

single-layer DLC foils irradiated by linearly polarized laser pulses are also shown in Fig. 3(b). One can see that their maximum C^{6+} energies are significantly lower than those using double-layer targets for all the cases.

To reveal the dependency of the ion energy on laser intensity, simulations were performed by varying the laser intensity. The maximum carbon energies obtained from the simulations are shown in Fig. 4 as the solid and dashed lines, where the laser energy is calculated as $\epsilon_{\text{laser}}(\text{J}) = 1.69 \times I_0(\text{W}/\text{cm}^2)/10^{20}$ according to the relationship between intensity and laser energy in our experiments. The solid line is obtained at the optimal thickness of the CNF for different intensities with a fixed CNF density of $0.2n_c$. The dashed line is obtained by scaling up the density of the CNF with laser intensity as well. It can be seen that the carbon energy is higher in the latter case, following $E_{\text{max}} \propto I^{0.6}$. This scaling is superior to TNSA but inferior to RPA. By comparing with existing RPA and TNSA results, one can speculate that for the laser intensity available now and in the near future, the cascaded acceleration would be a realistic optimal scheme for the generation of highly energetic heavy ions. It should be noted that the scaling obtained from carbon ions may not be directly applied to very heavy ions like Cu and Au, since the detailed ionization dynamics is not taken into account here. But the advantages of cascaded acceleration will be sustained. In addition to the study performed here, the dependence of ion spectra on the polarization of laser pulses needs to be explored further.

In summary, we demonstrate that cascaded laser acceleration of carbon ions can be achieved by combining a tens-of-micrometer-thick, slightly underdense plasma layer with

a nanometer-thin foil. The subsequent interplay of RPA and sheath acceleration leads to substantially higher maximum ion energy. This scheme is especially suited for heavy ion acceleration at realistic laser parameters currently accessible.

The work has been supported by the Institute for Basic Science of Korea under IBS-R012-D1, the National Basic Research Program of China (Grants No. 2013CBA01502 and No. 11475010), NSFC (Grants No. 11535001, No. 11775010, No. 61631001, and No. 11605111), and National Grand Instrument Project (No. 2012YQ030142). J. Q. Y. acknowledges the Projects No. 2016M600007 and No. 2017T100009 funded by China Postdoctoral Science Foundation. The particle-in-cell code EPOCH was in part funded by the UK EPSRC Grant No. EP/G054950/1. Our simulations were carried out at the Max Planck Computing and Data Facility and Shanghai Super Computation Center. J. S. and W. J. M. acknowledge support by the DFG-funded MAP cluster and the LMU target factory.

W. J. M. and I. J. K. contributed equally to the experiments in this work.

*Corresponding author.

wenjun.ma@pku.edu.cn

†Present address: Division of Scientific Instrumentation, Korea Basic Science Institute (KBSI), Daejeon 34133, Korea.

‡Corresponding author.

x.yan@pku.edu.cn

§Corresponding author.

chnam@gist.ac.kr

- [1] S. E. Woosley, *Nat. Phys.* **3**, 832 (2007).
- [2] D. Habs, P. G. Thirolf, M. Gross, K. Allinger, J. Bin, A. Henig, D. Kiefer, W. Ma, and J. Schreiber, *Appl. Phys. B* **103**, 471 (2011).
- [3] H. Daido, M. Nishiuchi, and A. S. Pirozhkov, *Rep. Prog. Phys.* **75**, 056401 (2012).
- [4] A. Macchi, M. Borghesi, and M. Passoni, *Rev. Mod. Phys.* **85**, 751 (2013).
- [5] L. Yin, B. J. Albright, K. J. Bowers, D. Jung, J. C. Fernandez, and B. M. Hegelich, *Phys. Rev. Lett.* **107**, 045003 (2011).
- [6] D. Jung *et al.*, *Phys. Plasmas* **20**, 083103 (2013).
- [7] A. Henig *et al.*, *Phys. Rev. Lett.* **103**, 045002 (2009).
- [8] S. Palaniyappan, C. Huang, D. C. Gautier, C. E. Hamilton, M. A. Santiago, C. Kreuzer, A. B. Sefkow, R. C. Shah, and J. C. Fernandez, *Nat. Commun.* **6**, 10170 (2015).
- [9] I. J. Kim *et al.*, *Phys. Plasmas* **23**, 070701 (2016).
- [10] A. Henig *et al.*, *Phys. Rev. Lett.* **103**, 245003 (2009).
- [11] S. Kar *et al.*, *Phys. Rev. Lett.* **109**, 185006 (2012).
- [12] S. Steinke *et al.*, *Phys. Rev. ST Accel. Beams* **16**, 011303 (2013).
- [13] J. Braenzel, A. A. Andreev, K. Platonov, M. Klingsporn, L. Ehrentraut, W. Sandner, and M. Schnurer, *Phys. Rev. Lett.* **114**, 124801 (2015).
- [14] M. Nishiuchi *et al.*, *Phys. Plasmas* **22**, 033107 (2015).
- [15] J. Fuchs *et al.*, *Nat. Phys.* **2**, 48 (2006).

- [16] A. Macchi, F. Cattani, T. V. Liseykina, and F. Cornolti, *Phys. Rev. Lett.* **94**, 165003 (2005).
- [17] T. Esirkepov, M. Yamagiwa, and T. Tajima, *Phys. Rev. Lett.* **96**, 105001 (2006).
- [18] J. Schreiber *et al.*, *Phys. Rev. Lett.* **97**, 045005 (2006).
- [19] B. M. Hegelich, B. J. Albright, J. Cobble, K. Flippo, S. Letzring, M. Paffett, H. Ruhl, J. Schreiber, R. K. Schulze, and J. C. Fernández, *Nature (London)* **439**, 441 (2006).
- [20] J. Schreiber *et al.*, *Appl. Phys. B* **79**, 1041 (2004).
- [21] B. M. Hegelich *et al.*, *Phys. Plasmas* **12**, 056314 (2005).
- [22] F. Wagner *et al.*, *Phys. Rev. Lett.* **116**, 205002 (2016).
- [23] C. Scullion *et al.*, *Phys. Rev. Lett.* **119**, 054801 (2017).
- [24] B. Qiao, S. Kar, M. Geissler, P. Gibbon, M. Zepf, and M. Borghesi, *Phys. Rev. Lett.* **108**, 115002 (2012).
- [25] A. V. Korzhimanov, E. S. Efimenko, S. V. Golubev, and A. V. Kim, *Phys. Rev. Lett.* **109**, 245008 (2012).
- [26] M. Chen, A. Pukhov, Z. M. Sheng, and X. Q. Yan, *Phys. Plasmas* **15**, 113103 (2008).
- [27] C. A. Palmer *et al.*, *Phys. Rev. Lett.* **108**, 225002 (2012).
- [28] H. Y. Wang, X. Q. Yan, J. E. Chen, X. T. He, W. J. Ma, J. H. Bin, J. Schreiber, T. Tajima, and D. Habs, *Phys. Plasmas* **20**, 013101 (2013).
- [29] J. H. Bin *et al.*, *Phys. Rev. Lett.* **115**, 064801 (2015).
- [30] B. Liu, H. Y. Wang, J. Liu, L. B. Fu, Y. J. Xu, X. Q. Yan, and X. T. He, *Phys. Rev. Lett.* **110**, 045002 (2013).
- [31] S. P. D. Mangles *et al.*, *Phys. Rev. Lett.* **94**, 245001 (2005).
- [32] A. Pukhov and J. Meyer-ter-Vehn, *Phys. Rev. Lett.* **76**, 3975 (1996).
- [33] A. V. Arefiev, V. N. Khudik, A. P. L. Robinson, G. Shvets, L. Willingale, and M. Schollmeier, *Phys. Plasmas* **23**, 056704 (2016).
- [34] T. W. Jeong, P. K. Singh, C. Scullion, H. Ahmed, K. F. Kakolee, P. Hadjisolomou, A. Alejo, S. Kar, M. Borghesi, and S. Ter-Avetisyan, *Rev. Sci. Instrum.* **87**, 083301 (2016).
- [35] W. Ma *et al.*, *Nano Lett.* **7**, 2307 (2007).
- [36] W. J. Ma, V. K. Liechtenstein, J. Szerypo, D. Jung, P. Hilz, B. M. Hegelich, H. J. Maier, J. Schreiber, and D. Habs, *Nucl. Instrum. Methods Phys. Res., Sect. A* **655**, 53 (2011).
- [37] See Supplemental Material at <http://link.aps.org/supplemental/10.1103/PhysRevLett.122.014803> for the details about the targets, and the energy distribution among laser, electrons and ions obtained from simulation results.
- [38] T. D. Arber *et al.*, *Plasma Phys. Controlled Fusion* **57**, 113001 (2015).
- [39] A. P. L. Robinson, A. V. Arefiev, and D. Neely, *Phys. Rev. Lett.* **111**, 065002 (2013).
- [40] I. J. Kim *et al.*, *Phys. Rev. Lett.* **111**, 165003 (2013).
- [41] F. Sylla, A. Flacco, S. Kahaly, M. Veltcheva, A. Lifschitz, G. Sanchez-Arriaga, E. Lefebvre, and V. Malka, *Phys. Rev. Lett.* **108**, 115003 (2012).
- [42] I. Prencipe *et al.*, *Plasma Phys. Controlled Fusion* **58**, 034019 (2016).
- [43] A. Sgattoni, P. Londrillo, A. Macchi, and M. Passoni, *Phys. Rev. E* **85**, 036405 (2012).